A Study of the Filter Properties of Single and Parallel-Coupled Dielectric-Waveguide Gratings

GEORGE L. MATTHAEI, FELLOW, IEEE, DONG CHUL PARK, STUDENT MEMBER, IEEE, YUN MYUNG KIM, AND DERON L. JOHNSON, STUDENT MEMBER, IEEE

Abstract—**Our work with gratings in dielectric image guide shows that it is distinctly advantageous to place the grating notches on the sides of the guide, or on the top of the guide, depending on the mode used. Means are discussed for modeling gratings using an equal-line-length transmission-line equivalent circuit. Excellent agreement between computed and measured bandstop frequency responses of gratings are obtained. Design relations for gratings are presented, and equations for analysis and design of parallel-coupled grating structures are derived. It is shown that a simple bandpass filter can be made from properly designed parallel-coupled gratings with distributed loads at one end. It is also shown that by use of combinations of parallel-coupled and direct-coupled gratings, multiresonator filters with Chebyshev or other characteristics can be obtained. Experimental results in agreement with computed responses are demonstrated.**

I. INTRODUCTION

BECAUSE OF THEIR potential value for millimeter-wave or optical integrated circuits, a great deal of research has been done on a variety of configurations of dielectric waveguides. However, relatively little has been done on techniques for realizing circuitry utilizing such a waveguide. This is particularly true in the case of dielectric-waveguide (DW) filters, which pose special problems. Since the energy is only loosely bound to most DW's, sharp bends will radiate strongly, *T*-junctions cannot be used, and open and short circuits are usually not available. This means that in most cases quite different design methods are required for DW filters than those which are normally used at microwave frequencies. An exception to the above statements occurs in the case of the "nonradiative" dielectric waveguide discussed in [12] and [13] which uses a dielectric guide between two metal ground planes. In this case, the "nonradiative mode" will not radiate as long as the frequency is below the frequency for which the spacing of the ground planes is $\lambda_{air}/2$. For such frequencies, sharp bends and *T*-junctions can be utilized. (There are also additional frequency bandwidth limitations related to the cutoffs of the fundamental and higher order nonradiative modes.) This guide presents some promising circuit possibilities, but its requirement of two metal ground planes and/or its frequency bandwidth limitations can be disadvantageous in some applications.

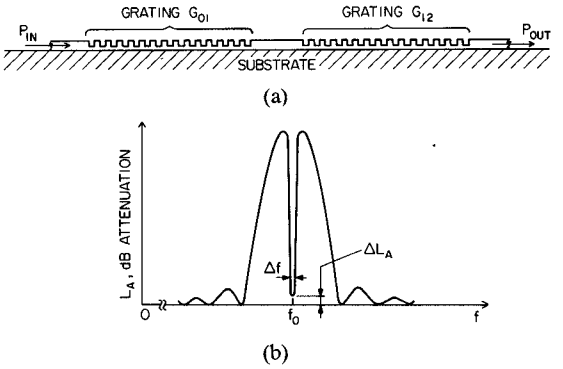

Fig. 1. (a) A two-port resonator in dielectric waveguide. (b) Typical attenuation characteristic for structure at (a).

There are a few DW filter structures which have appeared which are of practical interest. One is the DW grating which is well known to have useful potential for bandstop filter applications [1], but relatively little information is presently available in the literature to aid in the practical design of such gratings. Pairs of such gratings on a single guide, as in Fig. 1(a), can give a bandpass resonance centered in the stopband of the gratings as suggested in Fig. 1(b). This can be useful for frequency control of oscillators [2], but is useless for most bandpass filter applications because the width of the grating stopband would, in practical cases, be typically less than 10 percent. Until recently, the most practical DW bandpass filter that has been treated in the literature is the ring resonator filter [3]. However, this filter type has a major drawback in that, in order to reduce radiation, the DW ring must have a very sizeable radius as compared to a wavelength. This results in quite closely spaced passbands which are unacceptable for most situations of interest. Filters using the nonradiative guide [12], [13] mentioned above may provide attractive means for designing compact dielectric waveguide filters using techniques analogous to those used in TEM-mode stripline filters. However, the application of such filters will

Manuscript received March 8, 1983; revised April 26, 1983. This work was supported by the National Science Foundation under Grant ECS-8016720.

Y. M. Kim is with the Electronics Department, Dankook University, Seoul, Korea.

G. L. Matthaei, D. C. Park, and D. L. Johnson are with the Department of Electrical and Computer Engineering, University of California, Santa Barbara, CA 93106.

0018-9480/83/1000-0825$01.00 ©1983 IEEE

be limited by the two ground plane requirements, and by the bandwidth limitations of this type of guide (which may make it difficult to achieve stopbands as broad and strong as are frequently required).

We have been working on new ways of utilizing DW gratings in parallel-coupled configurations in order to obtain bandpass filters with strong broad stopbands. The methods used appear to be amenable to use with various forms of dielectric waveguides. Some early, preliminary results on this work have been previously reported [4], [5]. In order to build a sound basis for the optimum design of DW filters of this class, we have studied the fundamental properties of both single and parallel-coupled DW gratings. This paper reports on the results of that study. Herein, we will also discuss and illustrate by theoretical and experimental results how parallel-coupled grating structures can be used for realizing bandpass DW filters with broad stopbands. However, we will delay discussion of the systematic design of such filters for a future paper when more examples have been explored.

II. Configuration and Modeling of DW Gratings

We have been working with an "image guide" consisting of a DW on a metal ground plane, and have tested grating performance both using notches in the top of the guide as suggested in Fig. 1(a) and notches in the sides of the guide as indicated in Fig. 2(a). We found that when using the lowest order mode whose E field is predominantly vertically polarized (it would be referred to as the E_{11}^{y} mode in [6]), the use of notches on the sides of the guide as in Fig. 2(a) was decidedly superior [7]. Conversely, when using the predominantly horizontally polarized E_{11}^{x} mode, notches in the top of the guide as in Fig. 1(a) were much superior. By being "superior" we mean having a much stronger attenuation for the given depth of notches and having no spurious stopbands close to the desired stopband. In our filter tests, we have used the E_{11}^{y} mode and gratings with notches on their sides. These matters are discussed in [7] along with other observations concerning modes in DW gratings.

For purposes of a filter design using gratings, it is important to have an accurate, simple means for characterizing the gratings. As has been done by others, we model DW gratings by a transmission-line equivalent such as that in Fig. 2(b). But note that here the equivalent circuit uses line sections which are specifically all of the same length (and it assumes the same wave velocity throughout). By analysis of the circuit in Fig. 2(b) it can be shown that if a grating is terminated in Z_0 at both ends, the mid-stopband attenuation $A_{\max}$ in decibels is given by

$$A_{\max} = -10\log_{10}\left[\frac{4r^{2n}}{(r^{2n}+1)^2}\right] \text{dB} \tag{1}$$

where n is the number of Z_1 sections in the grating, and

$$r = \frac{Z_1}{Z_0} > 1 \tag{2}$$

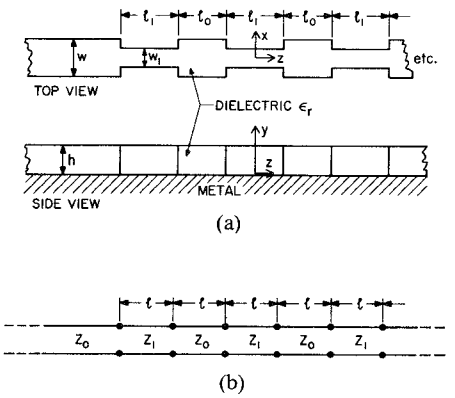

Fig. 2. (a) The dielectric-waveguide (DW) grating configuration used in the experiments in this paper. (b) An equal-line-length equivalent circuit for gratings such as that at (a).

which, as indicated, is greater than one for a grating such as that in Fig. 2(a). Equations (1) and (2) can be turned around so that we can compute r from a measured value of $A_{\max}$ for a test grating.[1] The result is

$$r = \sqrt[2n]{\frac{1+\sqrt{1-T}}{1-\sqrt{1-T}}} \tag{3a}$$

where

$$T = \text{antilog}_{10}\left(\frac{-A_{\max}}{10}\right). \tag{3b}$$

Thus the equivalent-circuit parameters for a given grating design can be determined experimentally by fabricating a trial grating and determining its mid-stopband attenuation $A_{\max}$ and the frequency f_0 at which that attenuation occurs. From n and the measured $A_{\max}$, r can be computed by (3a). The measured stopband center frequency f_0 fixes the wave velocity to be used in the equivalent circuit in Fig. 2(b) because at frequency f_0 all of the line lengths in the equivalent circuit are a quarter-wavelength long. Note that a more precise equivalent circuit than that in Fig. 2(b) would include lumped reactances to account for the fringing fields at the steps in Fig. 2(a). However, using the approach outlined here these effects are not ignored as we are using *effective* values of the impedance ratio $r = Z_1/Z_0$ and *average* wave velocity, both of which have the influence of these fringing fields merged into them. As we shall see, since the fringing field effects are relatively small, this approximate methods works quite well, at least for computing responses over the stopband frequencies.

Of course, dispersion must also be included for precise calculation of frequency response. Our approach has been to first obtain a measured wave velocity at the center frequency f_0 as described above. Then a theoretical average velocity at frequency f_0 over a period $l_0 + l_1$ in Fig. 2(a) is computed using the effective dielectric constant method [8]

[1] In our experimental work we measured $A_{\max}$ from measured responses such as that in Fig. 3(a) by drawing a horizontal line across between the minimum attenuation points on both sides of the stopband and then measuring from this line down to the maximum attenuation point.

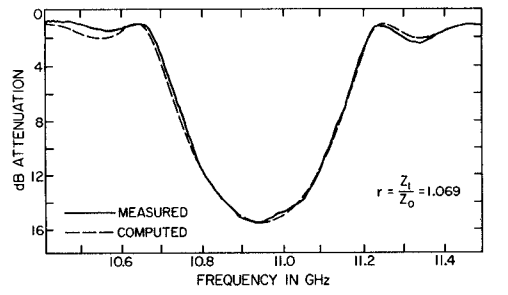

(a)

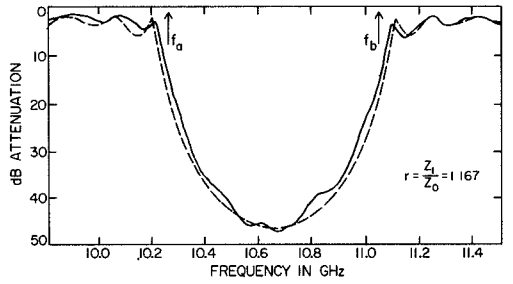

(b)

Fig. 3. (a) Computed and measured attenuation for a grating as in Fig. 2(a) with 35 narrow sections, $w = 1.270$ cm, $h = 1.016$ cm, $w_1/w = 0.625$, $l_0 = 0.528$ cm, $l_1 = 0.577$ cm, and $\epsilon_r = 2.55$. (b) Computed and measured attenuation for a grating as for Fig. 3(a) but with 38 narrow sections, $w_1/w = 0.375$, $l_0 = 0.541$ cm, and $l_1 = 0.648$ cm.

with junction fringing-field effects neglected.[2] Then the velocity used for computing the response is made to vary with frequency about the measured value at f_0 proportionally to the way the "theoretical" average velocity varies about its f_0 value.

Fig. 3(a) shows a measured response for a Rexolite 1422 grating as in Fig. 2(a) having $\epsilon_r = 2.55$, 35 Z_1 sections, and $w_1/w = 0.625$. (Detailed dimensions are given in the figure caption.) This grating was found to have $r = 1.069$, and the agreement between measured and computed responses is seen to be excellent. Fig. 3(b) shows the results for another grating made from the same material but with $w_1/w = 0.375$, giving very deep notches. In this case, the attenuation is much stronger and $r = 1.167$. Even though the fringing field effects in this case must be relatively large, the agreement between the measured and computed responses is still reasonably good.

In the example designs discussed above, we endeavored to make the electrical lengths of the Z_1 and Z_0 sections approximately equal at the stopband center frequency f_0, in conformity with the equivalent circuit in Fig. 2(b). However, we have found that in many situations one can use the equal-line-length circuit in Fig. 2(b) to accurately compute the frequency response for gratings where the Z_1 and Z_0 sections have very different electrical lengths. The requirements are that the effective value of r used in the circuit in Fig. 2(b) must be chosen to give the same midband attenuation as is given by the actual grating with unequal line electrical lengths, and the value of r must not be too large if the electrical lengths are very unequal. Taking an extreme example, the frequency response was computed for a grating having 30 Z_1 and Z_0 sections, $r = 1.2$, and a 1-to-3 ratio of line lengths. This grating had a midband attenuation of 27.6 dB. By (3a,b), the corresponding value of r for an equal-line-length model was $r = 1.138$, and the equal line lengths were set to the average value of the unequal line lengths. The frequency response for the equal-line-length model was very nearly the same as that for the unequal-line-length model in the vicinity of the stopband (where the computations were made). Being able to use this simple, equal-line-length model in Fig. 2(b) provides considerable simplification and convenience as fewer parameters are involved.

Besides experimental means for determination of the grating impedance ratio r, we have also investigated the use of the approximate equation

$$r = \frac{Z_1}{Z_0} \approx (v_p)_1/(v_p)_0 \tag{4}$$

where $(v_p)_1$ is the phase velocity in the region of Z_1 and $(v_p)_0$ is the phase velocity in the region of Z_0. Equation (4) would be exact for a metal waveguide carrying a TE mode with Z_0 regions completely filled with dielectric and Z_1 regions completely filled with air. Using the effective dielectric constant method for computing the velocities, (4) yields $r = 1.075$ for the grating used for Fig. 3(a) as compared to the 1.069 measured value. For the grating used for Fig. 3(b), (4) yields $r = 1.173$ as compared to the 1.167 measured value. This agreement is surprisingly good and shows that (4) can be a useful approximation for gratings, as in Fig. 2(a), excited in the E_{11}^y mode. However, we also found that in the case of an E_{11}^x mode exciting a grating as in Fig. 2(a), or an E_{11}^y mode exciting a grating made using notches in the top of the guide, the measured value of r is considerably less than is predicted by (4).

III. Characterization of Infinite Gratings

In order to be able to evaluate the fundamental characteristics of gratings independently from whatever terminations they are going to have, it is desirable to utilize the parameters of infinitely long gratings. This can be done in terms of their "image parameters" (see [10, ch. 3]). Fig. 4(a) shows part of a grating as in Fig. 2(b) which extends to infinity on the right. This infinite grating can be thought of as consisting of basic sections as in Fig. 4(b) with Z_0 ends connected to Z_0 ends and Z_1 ends connected to Z_1 ends. If we look in to the grating at the point Z_{I0} in Fig. 4(a), the impedance of the infinite grating extending to the right is given by

$$Z_{I0} = Z_0 \sqrt{\frac{(1+r)\cos\theta - (1-r)}{(1+r)\cos\theta + (1-r)}}\,. \tag{5a}$$

[2]This approximate theoretical average velocity has been around 3-percent lower than our measured average velocity in our example grating cases. Comparing these results with an average velocity obtained from velocities measured on sections of uniform guide suggests that most of the roughly 3-percent error referred to is due to the effective dielectric constant method approximations while surprisingly little error is due to the fringing fields at the discontinuities.

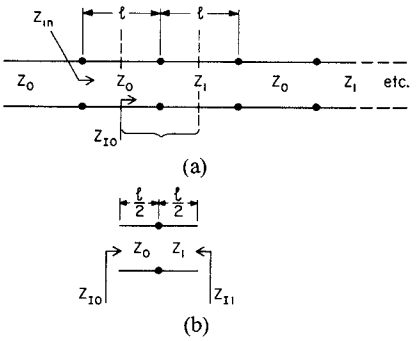

Fig. 4. (a) Equivalent circuit for a grating which extends to infinity to the right. (b) A fundamental section of the infinite grating.

Alternatively, if we look in to one of the basic sections as in Fig. 4(b) from the right side and the grating extends to infinity to the left, the impedance seen will be

$$Z_{I1} = Z_1 \sqrt{\frac{(1+r)\cos\theta + (1-r)}{(1+r)\cos\theta - (1-r)}} \tag{5b}$$

where

$$\theta = \frac{\pi f}{2f_0}. \tag{5c}$$

In (5c), f_0 is the frequency at which the line lengths l in Fig. 4(a) are a quarter-wavelength long. Of course, in many cases it will be necessary to modify the electrical-length relation (5c) in order to include the effects of dispersion. The impedances Z_{I0} and Z_{I1} are the "image impedances" for this structure and can be derived by the methods of [10, sec. 3.05]. When (5a) and (5b) are imaginary, the sign for the square root should be chosen so the reactance versus frequency has a positive slope.

Fig. 5(a) shows a plot of the image impedance Z_{I0} versus frequency for the exaggerated case of $r = 1.894$. Within the frequency range shown there is a passband from $f = 0$ to f_a and from f_b to $2f_0$, in which the impedance is purely real. Also there is a stopband from $f = f_a$ to f_b in which the impedance is purely imaginary. Now the impedance Z_{in} in Fig. 4(a) would usually be the one of most interest rather than Z_{I0}. If we add on the additional line length $l/2$ and compute the impedance Z_{in}, the result is as shown in Fig. 5(b). Note that in the stopband the grating exhibits series resonance. The sharp spurs in the X_{in} characteristic are possible because the grating is infinite.

By use of (5a)–(5c) it can be shown that the fractional bandwidth of the stopband of a grating is given by

$$\frac{\Delta}{f_0} = \frac{f_b - f_a}{f_0} = \frac{4}{\pi}\sin^{-1}\left(\frac{r-1}{r+1}\right) \tag{6a}$$

or for $(r-1) \ll 1$

$$\approx \frac{2}{\pi}(r-1)\Big|_{(r-1)\ll 1}. \tag{6b}$$

Note that for $(r-1) \ll 1$, the fractional stopband width is proportional to $(r-1)$. Equations (6a) and (6b) do not include the effects of dispersion, but at least for narrow-

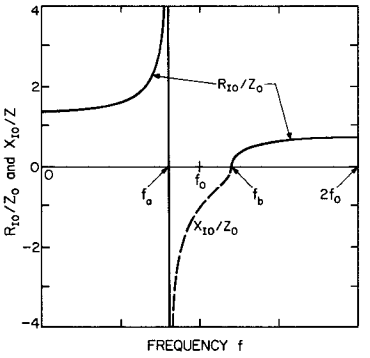

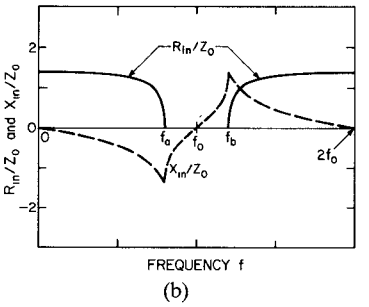

Fig. 5. (a) The image impedance Z_{I0} seen looking right into the infinite grating as defined in Fig. 4(a). (b) The impedance Z_{in} looking into the infinite grating as defined in Fig. 4(a).

band cases this can be corrected relatively simply by including appropriate derivatives of the guide wavelength. The above equations for Δ/f_0 should be divided by

$$D = -\left[\frac{l_0\frac{d\lambda_{g0}}{df} + l_1\frac{d\lambda_{g1}}{df}}{l_0\frac{\lambda_{g0}}{f} + l_1\frac{\lambda_{g1}}{f}}\right]_{f=f_0} \tag{7}$$

where l_0 and λ_{g0} are for the lines of impedance Z_0, and l_1 and λ_{g1} are for the lines of impedance Z_1. The parameter D is greater than one for dispersive gratings and reduces to one for nondispersive gratings. Thus it is seen that the effect of dispersion will be to reduce the stopband width.

The approximate values for the image-stopband-edge frequencies f_a and f_b are shown in Fig. 3(b) for that particular grating. If that grating was properly terminated in its image impedance at both ends, the attenuation would go identically to zero at f_a and f_b, and remain zero throughout the passbands. However, due to mismatch between the image impedance Z_{I0} and the Z_0 line impedances used at both ends, the attenuation does not go to zero at f_a and f_b, and has ripples in the passbands. The ripple minima occur when the overall image phase shift of the grating is a multiple of π so that the reflections from the ends cancel, while at the ripple maxima the overall image phase shift of the grating is an odd multiple of $\pi/2$ so that the reflections from the ends add in phase (see [10, ch. 3]).

By taking the derivative of the image reactance X_{I0} at f_0 (as in [9]), we find that the slope of X_{I0} at f_0 is like that of a line of impedance Z_0 which has total reflection at a point

$$m_d = \frac{1}{2(r-1)} + \frac{1}{2} = \frac{r}{2(r-1)} \tag{8}$$

half-wavelengths beyond where Z_{in} is observed in Fig. 4(a). (This equation differs from [9, (10b)] by 1/2 because Z_{in} looks into an initial Z_0 section instead of an initial Z_1 section.) For characterizing resonances such as that in Fig. 5(b) for purposes of filter design [10], it is useful to define a reactance slope parameter

$$x_{in} = \frac{\omega_0}{2} \frac{dX_{in}}{d\omega}\bigg|_{\omega=\omega_0}. \tag{9}$$

Making use of (8) and known properties of transmission-line resonators (see [10, sec. 5.08]), we find that the reactance slope parameter for the resonance of Z_{in} in Figs. 4(a) and 5(b) is given by

$$\frac{x_{in}}{Z_0} = \frac{\pi}{2} m_d. \tag{10}$$

This equation can be corrected for dispersion by multiplying by the factor D in (7). Equation (10) is applicable to finite as well as infinite gratings if the grating is long enough to have, say, 15-dB or more attenuation at f_0.

IV. Analysis of Parallel-Coupled Gratings

We shall see in Sections V–VII that parallel-coupled gratings have very useful properties for bandpass filter applications. When analyzing the coupling between such gratings, it is convenient to think in terms of their even and odd modes. The even mode is excited when the two gratings are driven symmetrically as suggested in Fig. 6(a), while the odd mode is excited if they are driven asymmetrically as shown in Fig. 6(c). Because of the symmetries, identical results are obtained for the left grating if it alone is used, and for the even mode a magnetic wall is placed at the plane of symmetry, while for the odd mode an electric wall is placed at that plane, as shown in Figs. 6(b) and 6(d). The effect of the magnetic wall or electric wall adjacent to the grating is primarily to alter the wave velocities in the grating. From test experiments we have found that for cases of very tight coupling the walls will also have significant effect on the $r = Z_1/Z_0$ ratio, but that in many cases of interest that effect is small and can be ignored. Thus we see that for the odd and even modes the gratings behave essentially the same except for somewhat different wave velocities. This will cause the stopbands for the odd and even modes to be centered at different frequencies.

Fig. 7(a) shows a pair of coupled gratings with a generator and load, and it will be of considerable use to us to obtain the transfer function V_2/V_g, where V_2 is the voltage between node 2 and ground. The excitation in Fig. 7(a) can be seen to be representable as a superposition of the even-mode excitation shown in Fig. 7(b) and the odd-mode

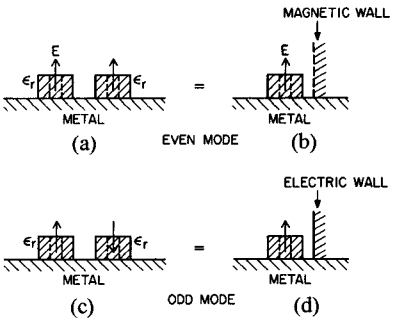

Fig. 6. At (a) is shown parallel gratings excited in the even mode and at (b) is shown an equivalent single-grating boundary-value problem. At (c) and (d) are shown analogous odd-mode situations.

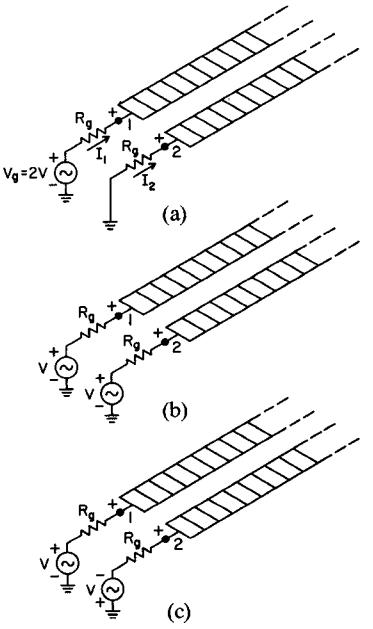

Fig. 7. At (a) is shown two coupled gratings driven by a single generator. This excitation is seen to be representable as the superposition of the even- and odd-mode excitations at (b) and (c), respectively.

excitation shown in Fig. 7(c). The even-mode reflection coefficient is

$$\Gamma^e = \frac{Z^e - R_g}{Z^e + R_g} = \frac{V_r^e}{V_i^e} \tag{11}$$

where Z^e is the impedance seen looking right from either node 1 or node 2 in Fig. 7(b) and V_i^e and V_r^e are the even-mode incident and reflected voltages, respectively. The impedance Z^e is computed from the transmission-line equivalent circuit using the average even-mode velocity v^e. (The even-mode velocities for the Z_0 and Z_1 sections will not be the same for a grating as in Fig. 2(a), so an average of the two velocities weighted in proportion to the lengths l_0 and l_1 (or a measured average value) should be used in the equal-line-length equivalent circuit.) The total even-mode voltage at terminal 1 is

$$V_1^e = V_i^e + V_r^e = \frac{V}{2} + \frac{V}{2}\Gamma^e. \tag{12}$$

Thus because of the symmetry of the even mode, at both nodes 1 and 2

$$V_2^e = V_1^e = \frac{V}{2}(1+\Gamma^e). \tag{13}$$

Analogously, for the odd-mode situation in Fig. 7(c) the reflection coefficient is

$$\Gamma^o = \frac{Z^o - R_g}{Z^o + R_g} \tag{14}$$

where Z^o is computed from the grating equivalent circuit using the average odd-mode velocity. Then by the odd-mode asymmetry

$$V_2^o = -V_1^o = -\frac{V}{2}(1+\Gamma^o). \tag{15}$$

The total voltage at node 2 is then

$$\begin{aligned} V_2 &= V_2^e + V_2^o \\ &= \frac{V}{2}(\Gamma^e - \Gamma^o) \end{aligned} \tag{16}$$

and our desired transfer function is

$$\frac{V_2}{V_g} = \frac{\Gamma^e - \Gamma^o}{4}. \tag{17}$$

Note that if

$$|\Gamma^e| = |\Gamma^o| = 1 \text{ and } \Gamma^e = -\Gamma^o \tag{18}$$

$|V_2/V_g| = 1/2$, and maximum power transfer will result. Inserting (11) and (14) in (17) yields

$$\frac{V_2}{V_g} = \frac{R_g(Z^e - Z^o)}{2(Z^e + R_g)(Z^o + R_g)}. \tag{19}$$

Equations (17) and (19) are specialized to the situation where the gratings have equal, resistive terminations R_g at ports 1 and 2. Cases having arbitrary circuits connected at the input and output can be treated by representing the coupled gratings using the well-known $ABCD$ parameters defined by

$$\begin{bmatrix} A & B \\ C & D \end{bmatrix} \begin{bmatrix} V_2 \\ -I_2 \end{bmatrix} = \begin{bmatrix} V_1 \\ I_1 \end{bmatrix} \tag{20}$$

where I_1 and I_2 are as defined in Fig. 7(a). It can be shown that

$$\begin{aligned} A = D &= \frac{Z^e + Z^o}{Z^e - Z^o} \\ B &= \frac{2Z^eZ^o}{Z^e - Z^o} \\ C &= \frac{2}{Z^e - Z^o}. \end{aligned} \tag{21}$$

It was noted herein that due to the different velocities for the odd and even modes, these modes have grating resonances at different frequencies. The question arises as to what velocity will fix the center frequency of a transmission resonance observed when the circuit is excited as in Fig. 7(a). Trying some simple examples, the effective phase constant for computing resonances is found to be

$$\beta_{\text{eff}} = \frac{\omega}{v_{\text{eff}}} = (\beta^e + \beta^o)/2 \tag{22}$$

where

$$v_{\text{eff}} = \frac{2v^ev^o}{v^e + v^o} \tag{23}$$

is the effective velocity. This effective velocity is used in calculating the center frequency f_0 of the passband which is provided by coupled gratings.

Equations (22) and (23) lead to convenient expressions for computing the even- and odd-mode electrical lengths in the equal-line-length models of the gratings. The even-mode electrical length for each line section is

$$\theta^e = \left(\frac{\pi(v^o/v^e)}{\frac{v^o}{v^e} + 1} \right) \frac{f}{f_0} \tag{24}$$

while each section electrical length for the odd mode is

$$\theta^o = \left(\frac{\pi}{\frac{v^o}{v^e} + 1} \right) \frac{f}{f_0} \tag{25}$$

where f_0 is the center frequency of the passband. (At f_0 all of the line sections are a quarter-wavelength long in terms of the wave velocity v_{eff}.)

V. A Simple Parallel-Coupled-Grating Bandpass Filter

Fig. 8 depicts a kind of DW grating structure which has useful bandpass filter properties. If properly designed, when the gratings are in their stopband, power entering at A will be transmitted on out port D. However, when the gratings are in their passbands, the power will be transmitted on to the loads on the right, and a stopband will exist with regard to transmission from port A to port D. It is important that as much as possible, coupling should only exist between the gratings and not between the input and output guides. This is because any power coupled directly between the input guide and the output guide will tend to reflect from the leading edge of the grating at D. This effect holds to some extent even when the gratings are in their passbands, and the small power reflected from the grating leading edge at D will degrade the stopband for transmission from the input to the output guide. Also, to minimize reflections from the right ends of the coupled guides, the loads are formed by gradually introducing lossy material into the grating structure. This is probably about as close as we can come to the ideal situation of terminating the gratings in their image impedances.

In order to analyze a structure of the sort in Fig. 8, let us first consider the idealized case in Fig. 9 which uses infinite gratings, with the leading edge of the coupled region at the center of a Z_0 section. Then Z^e and Z^o are given by (5a) using velocity v^e or v^o, respectively, and Z^e and Z^o both look like Fig. 5(a) but with a shift in frequency scales with

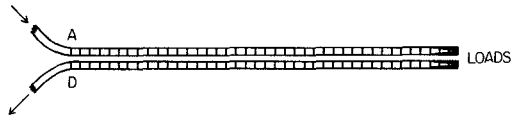

Fig. 8. A simple dielectric waveguide bandpass filter.

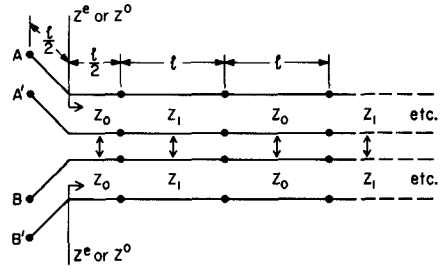

Fig. 9. Equivalent circuit for infinite coupled gratings with the first $l/2$ portion uncoupled.

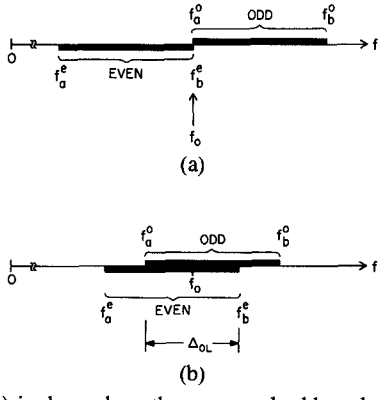

Fig. 10. At (a) is shown how the even- and odd-mode stopbands must be located in order to obtain complete power transfer at f_0 for the circuit of Fig. 8. At (b) is shown how these stopbands must overlap in order for the circuit in Fig. 14(b) to apply.

respect to each other. In order to get complete power transfer to the output guide, (18) must be satisfied. This condition will be fulfilled at f_0 if the velocities v^e and v^o are chosen so the even- and odd-mode stopbands are contiguous as shown in Fig. 10(a). Then frequency $f_a^o = f_0$ for which Z^o is infinite coincides with frequency f_b^e for which Z^e is zero, and by (11) and (14) we see that (18) is satisfied. By use of (5a) with $\theta^e = \omega l/v^e$ and $\theta^o = \omega l/v^o$, the stopband-edge constraint at f_0 in Fig. 10(a) gives

$$\frac{v^o}{v^e} = \frac{\cos^{-1}\left(\frac{1-r}{1+r}\right)}{\cos^{-1}\left(\frac{r-1}{r+1}\right)}. \tag{26}$$

This equation tells us that for a given grating impedance ratio r, in order to obtain complete power transfer at f_0 it is necessary that the gratings are spaced apart a distance so that the indicated average v^o/v^e ratio is achieved. Either closer or greater spacing will result in reduced power transfer.

Fig. 11 shows the computed response for the case of two infinite gratings having $r = 1.071$ which by (16) calls for

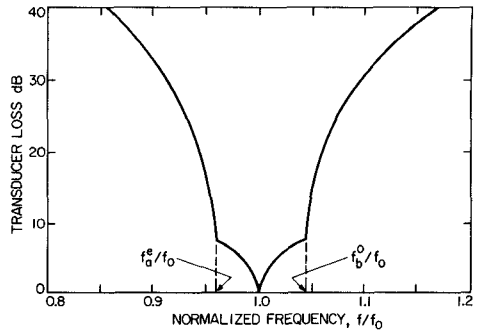

Fig. 11. Computed response for a filter design as in Fig. 8 with infinite gratings.

$v^o/v^e = 1.045$. The sharp corners in the response are possible because the gratings are infinite. Some analysis shows that the sharp breaks on the sides occur where

$$\frac{f_b^o}{f_0} = \frac{v^o}{v^e} \qquad \frac{f_a^e}{f_0} = \frac{v^e}{v^o}. \tag{27}$$

If, instead of starting the coupled region of the grating in the middle of a pair of Z_0 section (as suggested in Fig. 9), the coupled region is started at the beginning of a pair of Z_0 sections, then Z^e and Z^o will each look like Fig. 5(b), except for some difference in frequency scale. In this situation, for maximum power transfer at f_0, (18) must be satisfied by using a v^o/v^e ratio such that at f_0

$$jX_{\text{in}}^e\big|_{f=f_0} = jZ_0 = -jX_{\text{in}}^o\big|_{f=f_0}. \tag{28}$$

In most cases the bandwidths involved will not be very large and the v^o/v^e ratio obtained by (28) will be virtually the same as that obtained by (26).

A filter of the type in Fig. 8 was tested using a pair of gratings with the same parameters as for Fig. 3(a), spaced 0.610 cm apart, and driven in the E_{11}^y mode. The parallel-coupled gratings each had 32 Z_1 and Z_0 sections. Over about the last third of each grating, distributed loss was gradually introduced using absorbing foam material. The resulting response indicated by the solid line in Fig. 12 is seen to have the same V shape around the passband that is apparent in Fig. 11. The various minor spurs in the response result from the fact that the gratings are not terminated in their image impedance, and thus numerous weak resonances occur because of the small reflections at the ends of the gratings. We found that these resonances were greatly suppressed by use of loads formed by distributed loss in the gratings as for the solid line in Fig. 12. For example, the dashed line in Fig. 12 shows the computed response for the case in which the gratings are abruptly terminated in Z_0 loads. The distributed loads are seen to work much better.

The midband loss of 2.6 dB in Fig. 12 includes the mode launchers and about 86 cm of connecting DW waveguides. The midband loss of the filter structure alone is less than 1.5 dB. Note that the nominal stopband attenuation is at most frequencies 30 dB or better. Since this type of filter is absorptive in its stopbands it should be possible to cascade

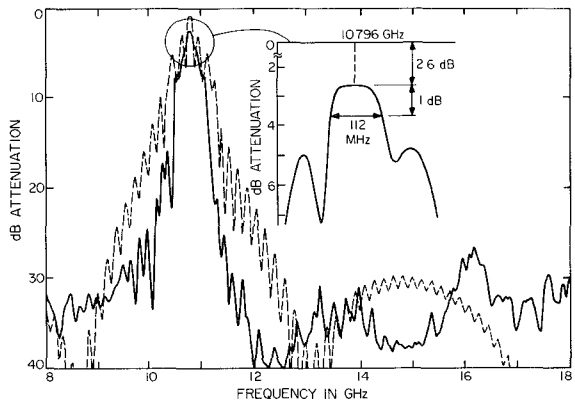

Fig. 12. The solid line shows a measured response (including mode transducers and connecting DW guides) for a filter as in Fig. 8 using distributed loads. The dashed line shows a computed response using lumped Z_0 loads.

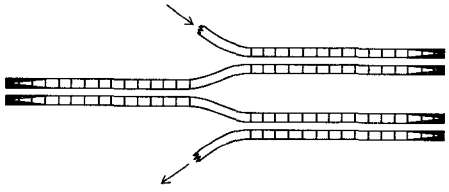

Fig. 13. Filters of the type in Figs. 8 and 12 cascaded to give very high stopband attenuation.

such structures without having harmful stopband interactions. Thus very large stopband attenuations may be possible using cascaded filters as in Fig. 13.

VI. The Impedance-Inverting Property of Parallel-Coupled Gratings

Suppose we have two resonators, each of which exhibits a series-type of resonance. If they are connected in series they will simply give a single-resonator response with an increased reactance slope parameter. In order to give a two-resonator type of response they must be coupled by a circuit which has an effect like the impedance inverter K_{12} in Fig. 14(b). (Recall that an idealized impedance inverter acts like a transmission line of characteristic impedance K_{12} with $\pm 90°$ phase shift at all frequencies.) Both of the gratings in Fig. 14(a) when isolated and viewed from the input of a full Z_0 section presents a series-type resonance similar to that in Fig. 5(b). If two such gratings are placed parallel to each other so that they interact, it is desirable to know if at terminals A and B in Fig. 14(a) they behave like the two-resonator equivalent circuit in Fig. 14(b) for frequencies in the vicinity of the desired passband; and if so, what the values are for the reactance slope parameters χ_1 and χ_2, and for the inverter parameter K_{12}, at the center

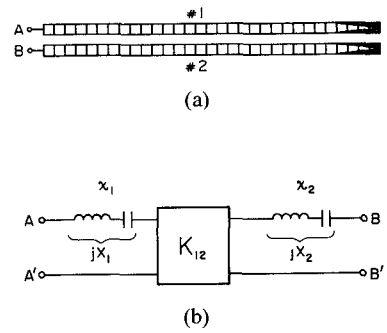

Fig. 14. At (b) is shown an equivalent circuit which applies for the circuit shown at (a) at frequencies for which the stopband-overlap condition in Fig. 10(b) is satisfied.

frequency f_0.

The A, B, C, D parameters for the circuit in Fig. 14(b) are

$$\begin{bmatrix} A_t & B_t \\ C_t & D_t \end{bmatrix} = \begin{bmatrix} -X_1/K_{12} & j(K_{12} - X_1X_2/K_{12}) \\ j/K_{12} & -X_2/K_{12} \end{bmatrix} \tag{29}$$

where at the resonant frequency f_0 of the resonators,

$$\begin{bmatrix} A_t & B_t \\ C_t & D_t \end{bmatrix}_{f=f_0} = \begin{bmatrix} 0 & jK_{12} \\ j/K_{12} & 0 \end{bmatrix}. \tag{30}$$

We wish to compare the A, B, C, D parameters for the circuit in Fig. 14(a) with those above in order to establish any equivalence that may exist.

In order to simplify the analysis we shall assume that the gratings are infinite and that they are coupled only up to the middle of the input Z_0 section as shown in Fig. 9. Then by (5a) Z^e and Z^o are given by

$$Z^e = Z_0\sqrt{\frac{(1+r)\cos\theta^e - (1-r)}{(r+1)\cos\theta^e + (1-r)}} \tag{31}$$

and

$$Z^o = Z_0\sqrt{\frac{(1+r)\cos\theta^o - (1-r)}{(1+r)\cos\theta^o + (1-r)}} \tag{32}$$

where θ^e and θ^o are given by (24) and (25). We actually wish to refer our equivalent circuit to the inputs of the first full Z_0 sections, so we need to add the input sections shown in Fig. 9. In our analysis we make the simplifying assumptions that these $l/2$ sections are not coupled and that their electrical length is frequency independent. Since these line lengths are only $\lambda/8$ at f_0, and since we are presently interested in parameters evaluated at f_0, this should cause little error.

Based on the above assumptions, the transmission parameters referred to the input terminals in Fig. 9 are given by

$$\begin{bmatrix} A_t' & B_t' \\ C_t' & D_t' \end{bmatrix} \approx \begin{bmatrix} \frac{1}{\sqrt{2}} & \frac{jZ_0}{\sqrt{2}} \\ j\frac{1}{Z_0\sqrt{2}} & \frac{1}{\sqrt{2}} \end{bmatrix} \begin{bmatrix} A & B \\ C & D \end{bmatrix} \begin{bmatrix} \frac{1}{\sqrt{2}} & \frac{jZ_0}{\sqrt{2}} \\ j\frac{1}{Z_0\sqrt{2}} & \frac{1}{\sqrt{2}} \end{bmatrix} \tag{33}$$

where A, B, C, and D are given by (21), (31), and (32). The equivalent circuit in Fig. 14(b) has no dissipation; hence, for frequencies for which the circuits in Figs. 14(a) and 14(b) are equivalent, both the grating even and odd modes must be in their stopbands as is suggested by the stopband overlap region Δ_{0L} in Fig. 10(b). In this band, $Z^e = jX^e$ and $Z^o = jX^o$, and the results of (33) are

$$A_t' = D_t' = \frac{Z_0^2 - X^e X^o}{Z_0(X^e - X^o)}$$

$$B_t' = \frac{j(Z_0 + X^o)(Z_0 + X^e)}{X^e - X^o}$$

$$C_t' = \frac{-j(Z_0 - X^o)(Z_0 - X^e)}{Z_0^2(X^e - X^o)}. \tag{34}$$

From (24) and (25) we find that at $f_0, \cos\theta^e = -\cos\theta^o$. Then by (31) and (32)

$$X^e X^o|_{f=f_0} = Z_0^2 \tag{35}$$

which causes $A_t' = D_t' = 0$ at f_0 just as for A_t and D_t in (30). Comparing C_t in (29) with C_t' in (34) gives

$$K_{12} = \frac{Z_0^2(X^o - X^e)}{(Z_0 - X^e)(Z_0 - X^o)}. \tag{36}$$

Using (35), at f_0 (36) can be simplified to

$$K_{12}|_{f=f_0} = Z_0\left(\frac{Z_0 + X^o}{Z_0 - X^o}\right)_{f=f_0}. \tag{37}$$

In order to compute the resonator slope parameters χ_1 and χ_2 for the coupled resonators we first need to determine the resonator equivalent reactances jX_1 and jX_2 in Fig. 14(b). Using A_t, C_t, and D_t from (29), and using the fact that $A_t = D_t$ because of the symmetry of the circuit, we find that

$$jX_1 = jX_2 = A_t/C_t. \tag{38}$$

Substituting A_t' and C_t' from (34) in this equation shows that

$$jX_1 = jX_2 = jZ_0\frac{(Z_0^2 - X^o X^e)}{(Z_0 - X^e)(Z_0 - X^o)} \tag{39}$$

for the coupled-gratings equivalent circuit. Note that due to (35), $jX_1 = jX_2 = 0$ at f_0 as should be the case. The resonator slope parameters χ_1 and χ_2 are easily computed numerically by use of (9), (39), (31), and (32).

VII. A Coupled-Resonator Filter Example

Without going into the design details at this time, a filter example will be presented which demonstrates the feasibility of coupled-resonator filters utilizing gratings. Fig. 15(a) shows a two-resonator filter, where each resonator consists of a pair of gratings, in a manner similar to the resonator in Fig. 1(a). The gratings are located on the guides so that the last Z_1 section of grating G_{01} on the upper guide is separated from the first Z_1 section of grating G on the upper guide by $\lambda_g/2$, and similarly for the resonator on the lower guide. It is important that gratings G_{01} and G_{23} not be coupled to each other for the same reason that it was important to keep the input guides separated for the example in Section V. The primary function of gratings G_{01} and G_{23} is to control the amount of termination loading seen by the resonators, but these gratings also contribute to the total resonator reactance slope parameters $(\chi_1)_{\text{total}}$ and $(\chi_2)_{\text{total}}$. Fig. 16 shows an equivalent circuit for the filter in Fig. 15(a) for frequencies near f_0, where the portion of the structure between A and B in Fig. 16 models the coupled gratings G in Fig. 15(a) by use of the equivalence in Fig. 14(a) and (b). The circuit to the left of A in Fig. 16 represents grating G_{01} and the source guide, while the circuit to the right of B represents grating G_{23} and the load guide. In the gratings G_{01}, G_{23}, the gratings G all have the same resonant frequency, and the overall effect in Fig. 16 is to give a two-resonator filter response.

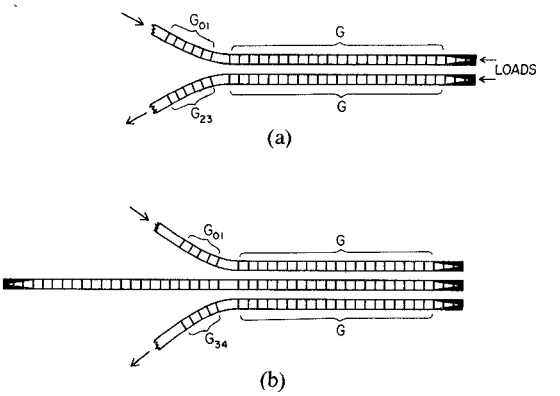

Fig. 15. At (a) is shown a two-resonator filter while at (b) is shown a three-resonator filter of the same type.

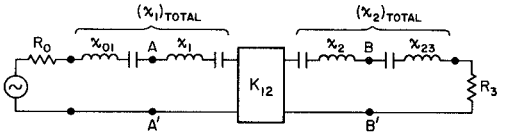

Fig. 16. An equivalent circuit for the filter in Fig. 15(a) for frequencies near f_0.

Using methods similar to those discussed in [11], a trial design was worked out for the Chebyshev response with 0.5-dB ripple, a fractional bandwidth of about 0.011 (ignoring dispersion), and a grating impedance ratio of $r = 1.07$. This design called for $v^o/v^e = 1.02$ for the coupled gratings G, and 13 Z_1 and Z_0 sections in gratings G_{01} and G_{23}. Using analysis methods discussed herein, the attenuation characteristic for this filter with infinite gratings G was computed, and this result is shown by the dashed curve in Fig. 17. A response was also computed for the more practical case of gratings G each with 47 lossless Z_1 and Z_0 sections, along with 21 more Z_1 and Z_0 sections with gradually increasing loss. (The loss was introduced by way of a dielectric loss factor which increased linearly from $\epsilon''/\epsilon' = 0.004$ to 0.084.) The results of these calculations are shown by the solid line in Fig. 17. These computed results indicate that this structure has quite promising bandpass filter properties.

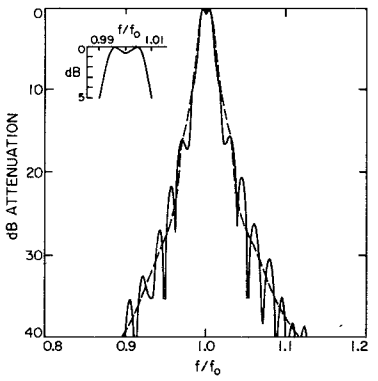

Fig. 17. The dashed line shows a computed response for a filter of the type in Fig. 15(a) with gratings G infinite. The solid curve shows a computed response for finite gratings G and distributed loads.

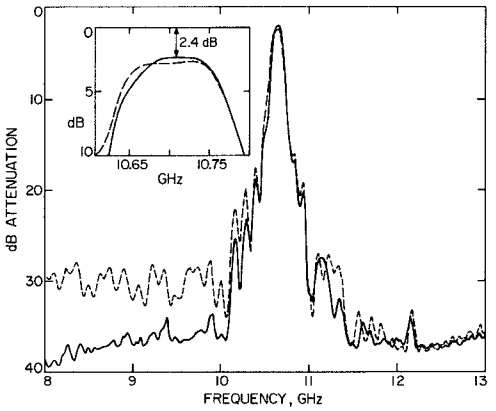

Fig. 18. The dashed line shows a measured response for a filter as in Fig. 15(a), while the solid line shows the response with a metal divider inserted between gratings G_{01} and G_{23}. The responses include mode transducers and connecting DW guides.

A trial filter based on the design discussed above was fabricated. It used gratings with notches on their sides with parameters the same as those for the grating for Fig. 3(a). Calculations indicated that for this design, if gratings G_{01} and G_{23} in Fig. 15(a) were replaced by uniform guides, the midband loss should be 6.3 dB. Thus we first operated the structure as shown in Fig. 8, and adjusted the grating spacings until the midband loss was 6.3 dB greater than that recorded in the measurements in Fig. 12. (The adjusted spacing was 1.14 cm.) Then the smooth input and output guides were replaced by guides each having 13 pairs of notches to form gratings G_{01} and G_{23}. In order to locate the resonator resonances at the center of the stopband of the gratings, we found it desirable to add some dielectric spacers in the joint between G_{01} and its adjacent G grating, and similarly between G_{23} and its adjacent G grating. (Due to fringing effects at the step junctions we had underestimated the required center-section length). Then the response indicated by the dashed curve in Fig. 18 was obtained (the 13- to 18-GHz range was similar to that in Fig. 12). This response has about 0.15-dB Chebyshev ripple, and is slightly mistuned as is indicated by its small tilt. We found that this error could be corrected by putting small pieces of dielectric material next to the guide at the center of each resonator (or it could have been corrected by altering the dielectric spacers). Since no attempt was made to include dispersion in the theoretical calculations in Fig. 17, no attempt was made to correlate the measured and computed responses precisely. However, note that in and around the passband the responses are qualitatively in good agreement.

In fabricating the filter structure in Fig. 15(a) we had anticipated possible trouble due to radiation from gratings G_{01} and G_{23} which were formed on curved sections of the guide. However, there were no indications that these gratings had introduced any significant radiation loss. We were also curious about possible effects due to unwanted stray coupling between the guides to the left of the grating G. A metal dividing wall with a sharp leading edge was inserted between gratings G_{01} and G_{23}. The measured response shown by the solid line in Fig. 18 was then obtained. Note that the stopband attenuation below the passband has been significantly increased, while the passband response no longer has a Chebyshev ripple, indicating slightly less coupling. The minimum loss is about 2.4 dB which includes the loss of the mode transducers and the input and output connecting DW guides. Again, the midband loss of the filter alone is less than 1.5 dB.

In [4], a multiresonator configuration using parallel-coupled gratings for coupling into the first and out of the last resonators is described. The configurations in Fig. 15(a) and (b) are probably preferable in most cases because of the relatively tight couplings required between the terminations and their adjacent resonators. The use of the direct-coupled gratings such as G_{01} and G_{23} in Fig. 15(a) permits a wide range of coupling to the terminations with no tolerance problems or possible distorted passband responses due to the even- and odd-mode grating stopbands not overlapping for terminating parallel gratings (as in [4]).

VIII. Conclusions

Relations and techniques for the analysis and design of DW single gratings and parallel-coupled gratings for filter applications have been obtained. The formulas which assume the use of infinite gratings should be particularly useful for design purposes. The filter type in Fig. 8 is quite simple and has attenuation characteristics which are adequate for many applications, especially if such filter sections are cascaded as shown in Fig. 13 to enhance the stopband attenuation level. However, the filter structures in Figs. 8 and 13 provide quite limited control of the passband characteristic. By use of coupled-resonator filter structures such as the two-resonator structure in Fig. 15(a), and the analogous three-resonator version in Fig. 15(b), Chebyshev, maximally flat, or other passband characteristics can be obtained. Still, other structural variations are possible which may have advantages.

References

[1] T. Itoh, "Application of gratings in a dielectric waveguide for leaky-wave antennas and band-reject filters," *IEEE Trans. Microwave Theory Tech.*, vol. MTT-25, pp. 1134–1138, Dec. 1977.

[2] T. Itoh and F.-J. Hsu, "Distributed Bragg reflector Gunn oscillators for dielectric millimeter-wave integrated circuits," *IEEE Trans. Microwave Theory Tech.*, vol. MTT-27, pp. 514–518, May 1979.
[3] R. M. Knox, "Dielectric waveguide microwave integrated circuits —An overview," *IEEE Trans. Microwave Theory Tech.*, vol. MTT-24, pp. 806–814, Nov. 1976.
[4] G. L. Matthaei, C. E. Harris, D. C. Park, and Y. Kim, "Dielectric-waveguide filters using parallel-coupled grating resonators," *Electron. Lett.*, vol. 18, pp. 509–510, June 10, 1982.
[5] G. L. Matthaei, C. E. Harris, Y. M. Kim, D. C. Park, and J. P. Duvall, "Simple dielectric waveguide bandpass filter," *Electron. Lett.*, vol. 18, pp. 798–799, Sept. 2, 1982.
[6] E. A. J. Marcatili, "Dielectric rectangular waveguide and directional coupler for integrated optics," *Bell Syst. Tech. J.*, vol. 48, pp. 2071–2102, Sept. 1969.
[7] G. L. Matthaei, "A note concerning modes in dielectric waveguide gratings for filter applications," *IEEE Trans. Microwave Theory Tech.*, vol. MTT-31, pp. 309–312, Mar. 1983.
[8] W. V. McLevige, T. Itoh, and R. Mittra, "New waveguide structures for millimeter-wave and optical integrated circuits," *IEEE Trans. Microwave Theory Tech.*, vol. MTT-23, pp. 788–794, Oct. 1975.
[9] G. L. Matthaei, B. P. O'Shaughnessy, and F. Barman, "Relations for analysis and design of surface-wave resonators," *IEEE Trans. Sonics Ultrason.*, vol. SU-23, pp. 99–107, Mar. 1976.
[10] G. L. Matthaei, L. Young, E. M. T. Jones, *Microwaves Filters, Impedance-Matching Networks, and Coupling Structures*. New York: McGraw-Hill, 1964; Dedham, MA: Artech House, 1980.
[11] G. L. Matthaei, E. B. Savage, and F. Barman, "Synthesis of acoustic-surface-wave-resonator filters using any of various coupling mechanisms," *IEEE Trans. Sonics Ultrason.*, vol. SU-25, pp. 72–84, Mar. 1978.
[12] T. Yoneyama and S. Nishida, "Nonradiative dielectric waveguide for millimeter-wave integrated circuits," *IEEE Trans. Microwave Theory Tech.*, vol. MTT-29, pp. 1188–1192, Nov. 1981.
[13] T. Yoneyama, M. Yamaguchi, and S. Nishida, "Bends in nonradiative dielectric waveguides," *IEEE Trans. Microwave Theory Tech.*, vol. MTT-30, pp. 2146–2150, Dec. 1982.

✤

George L. Matthaei (S'49–A'52–M'57–F'65), was born August 28, 1923, in Tacoma, WA. He received the B.S. degree from the University of Washington in 1948, and the Ph.D. degree from Stanford University, CA, in 1952.

From 1951 to 1955, he was on the faculty of the University of California, Berkeley, where he was an Assistant Professor, and his specialty was network synthesis. From 1955 to 1958, he was engaged in system analysis and microwave component research at the Ramo-Wooldridge Corporation. From 1958 to 1964, he was at Stanford Research Institute where he was engaged in microwave device research and became Manager of the Electromagnetic Techniques Laboratory in 1962. In July 1964, he joined the Department of Electrical Engineering at the University of California, Santa Barbara, where he is a Professor. He is the author of numerous papers, coauthor of the book *Microwave Filters, Impedance-Matching Networks and Coupling Structures*, and a contributor to several other books.

Dr. Matthaei is a member of Tau Beta Pi, Sigma Xi, and Eta Kappa Nu. He was the winner of the 1961 Microwave Prize of the IEEE MTT Group.

✤

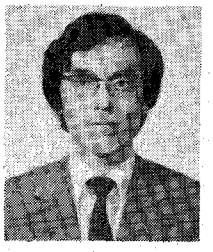

Dong Chul Park (S'81) was born in Pusan, Korea, in 1952. He received the B.S. degree in electronics from Seoul National University, Seoul, Korea, in 1974, and the M.S. degree in electronics from Korea Advanced Institute of Science and Technology (KAIST), Seoul, Korea, in 1976.

From 1976 to 1981, he worked at Chungnam National University, Daejon, Korea. From 1977 to 1978, he was a Visiting Scholar at Ruhr-University, Bochum, West Germany, where he worked on integrated optics. In 1981, he came to the University of California, Santa Barbara, on a Fulbright Grant. He is working toward the Ph.D. degree in electrical engineering. His research interests are in electromagnetic field theory, microwave and millimeter-wave devices, and integrated optics.

✤

Deron L. Johnson (S'81) was born in Santa Barbara, CA, on May 1, 1961. He is a candidate for a B.S. in electrical and computer engineering at the University of California, Santa Barbara, in June, 1983. His primary interests are microwave filter and antenna design.

Mr. Johnson is a member of Tau Beta Pi.

✤

Yun Myung Kim received the B.S. degree in electronics from the Seoul National University, Seoul, Korea, in 1975, and the M.S. degree in electronics from the Korea Advanced Institute of Science and Technology (KAIST), Seoul, Korea, in 1977.

After graduation he joined Goldstar Precision Company, where he was engaged in the radar development. Since 1980 he has been working as a faculty member at the Department of Electronics in Dankook University, Seoul, Korea, where he is presently an Assistant Professor. From 1982 to 1983 he was a Visiting Scholar at the University of California, Santa Barbara. His research interests are in electromagnetic field theory, microwave and millimeter-wave devices, and antennas.